INTERNATIONAL JOURNAL FOR NUMERICAL AND ANALYTICAL METHODS IN GEOMECHANICS
Int. J. Numer. Anal. Meth. Geomech., 2006; **30**:1579–1600
Published online 18 September 2006 in Wiley InterScience (www.interscience.wiley.com). DOI: 10.1002/nag.549

Effects of anisotropic permeability on stabilization and pore water pressure distribution of poorly cemented stratified rock slopes

Jia-Jyun Dong[1,*,†], Jian-Hou Tzeng[1], Po-Kai Wu[2] and Ming-Lang Lin[3]

[1] *Institute of Applied Geology, National Central University, No.300, Jungda Rd., Jungli, Taoyuan, Taiwan 320, R.O.C.*
[2] *Department of Construction Engineering, National Yunlin University of Science & Technology, Yunlin, Taiwan, R.O.C.*
[3] *Department of Civil Engineering, National Taiwan University, Taipei, Taiwan, R.O.C.*

SUMMARY

Slopes composed of stratified and poorly cemented rocks that fail during heavy rainfalls are typical in the outer zone of Taiwan's Western Foothills. This study investigates how hydraulic conductivity anisotropy influences pore water pressure (PWP) distributed in stratified, poorly cemented rock slopes and related slope stability through numerical simulation. The notion of representing thin alternating beds of stratified, poorly cemented rocks as an equivalent anisotropic medium for groundwater flow analysis in finite slopes was validated. PWP was then derived in a modelled slope comprising an anisotropic medium with suitable boundary conditions. Simulation results indicate the significance of the principal directions of hydraulic conductivity tensor and the anisotropic ratio on PWP estimation for anisotropic finite slopes. For a stratified, poorly cemented rock slope, estimating PWP utilizing a phreatic surface with isotropic and hydrostatic assumptions will yield incorrect results. Stability analysis results demonstrate that hydraulic conductivity anisotropy affects the slope safety factor and slip surface pattern. Consequently, steady-state groundwater flow analysis is essential for stratified, poorly cemented rock slopes when evaluating PWP distribution and slope stability. This study highlights the importance of hydraulic conductivity anisotropy on the stability of a stratified, poorly cemented rock slope. Copyright © 2006 John Wiley & Sons, Ltd.

Received 16 December 2005; Revised 23 June 2006; Accepted 13 July 2006

KEY WORDS: poorly cemented stratified rock slopes; pore water pressure; groundwater flow analysis; hydraulic conductivity anisotropy; slope stability

*Correspondence to: Jia-Jyun Dong, Institute of Applied Geology, National Central University, No. 300, Jungda Rd., Jungli, Taoyuan, Taiwan 320, R.O.C.
† E-mail: jjdong@geo.ncu.edu.tw

Contract/grant sponsor: National Science Council; contract/grant number: NSC-91-2211-E-008-024

INTRODUCTION

Gently warped and poorly cemented Pliocene to Pleistocene conglomerate, sandstone, siltstone, mudstone and shale are the dominant formations distributed throughout the outer zone of Taiwan's Western Foothills (hereafter called the outer foothill zone) [1]. Yen *et al*. [2] described several slope failures triggered by heavy rainfall during construction of a highway in the northern section of the outer foothill zone; these failed slopes are composed of stratified, poorly cemented sandstone, siltstone, mudstone and shale. Misfeldt *et al*. [3] identified that groundwater flow patterns and, thus, pore water pressures (PWP), distributed in slopes may dominate the slope-stability of active landslides. Therefore, evaluating the distribution of PWP in stratified and poorly cemented rock slopes is essential for mitigating the damage caused by landslides.

Three features are crucial when analysing groundwater flow and slope stability of stratified and poorly cemented rocks distributed in the northern section of the outer foothill zone. (1) The uniaxial compressive strengths of the poorly cemented rocks distributed in northern section of the outer foothill zone are typically < 5 MPa [4]. That is, the poorly cemented rocks are soil-like. (2) Faulting is not prevalent and folds are broad and gentle in outer foothill zone [5]. Consequently, the spacing of joints in most poorly cemented rocks is very wide. Since these poorly cemented rocks are soil-like, the stressed joints are usually sealed. Brace [6] concluded that fractures may have a minor hydrological role for certain argillaceous rocks and sandstone. Consequently, it is reasonable to assume that the groundwater flow in poorly cemented rock slopes is dominated by inter-granular flow and, hence, Darcy's law is valid. (3) Poorly cemented rocks in the northern section of the outer foothill zone are stratified and therefore heterogeneous. The principal values for hydraulic conductivity of sandstone and siltstone are $5\text{–}9 \times 10^{-5}$ and $1\text{–}10 \times 10^{-6}$ cm/s, respectively [7]. Sandstone and siltstone are somewhat hydraulically isotropic. On the other hand, for stratified shale and sandstone with thin alternation beds, the equivalently hydraulic conductivity parallel to the bedding plane is 10–150 times larger than that perpendicular to the bedding plane [7]. Therefore, the hydraulic conductivity of the stratified rocks is anisotropic, equivalently.

The effect of hydraulic conductivity heterogeneity on PWP distribution in a layered slope and the related slope stability has been investigated systematically by other studies [8–14]. The PWP distributed in a heterogeneous slope is significantly different from that in a homogeneous slope [8]. On the other hand, the effect of hydraulic conductivity anisotropy on PWP distribution of a slope and on the consequent slope stability has attracted scant attention. This study explores how hydraulic conductivity anisotropy influences PWP distributed in stratified, poorly cemented rock slopes and the related slope stability via numerical simulation. First, the distributed PWP in a stratified, heterogeneous medium and equivalent anisotropic medium are calculated based on two-dimensional groundwater flow analysis. In this manner the notion of using an equivalent anisotropic medium to represent a stratified heterogeneous medium is validated. Second, the PWP distributed in the modelled slopes with different anisotropic ratios of hydraulic conductivity and the inclined angles of stratification are compared. The influence of anisotropic hydraulic conductivity on the groundwater flow in a finite slope is demonstrated. Moreover, the validity in employing phreatic surfaces to determine PWP distribution of rock slopes with hydraulic conductivity anisotropy is evaluated. Finally, the influence of PWP—induced by hydraulic conductivity anisotropy—on the stability of stratified and poorly cemented rock slopes is elucidated.

DOI: 10.1002/nag

NUMERICAL MODEL FOR SIMULATING GROUND WATER FLOW IN FINITE SLOPES

Two-dimensional Darcian groundwater flow in a heterogeneous anisotropic medium

Darcy's law of seepage can be generalized in two- or three-dimensional scenarios [15]. For an anisotropic medium, the hydraulic-conductivity at a given point can be described using a symmetrical tensor, k_{ij}. Based on continuity relations and Darcy's law, the Laplace equation for steady two-dimensional groundwater flow in a saturated heterogeneous anisotropic medium is

$$\frac{\partial}{\partial x}\left(k_{xx}\frac{\partial h}{\partial x}+k_{yx}\frac{\partial h}{\partial y}\right)+\frac{\partial}{\partial y}\left(k_{xy}\frac{\partial h}{\partial x}+k_{yy}\frac{\partial h}{\partial y}\right)=0 \tag{1}$$

where h is the total hydraulic head, and $k_{xx}, k_{yx}=k_{xy}, k_{yy}$ are the components of the hydraulic conductivity tensor.

Figure 1 presents the adopted global and local co-ordinates (x, y and x', y') in which the local co-ordinate (x',y') is chosen to coincide with the principal directions of the hydraulic conductivity tensor. When the inclined angle of stratification θ between x and x' axes and the principal values $k_{x'}$ and $k_{y'}$ are specified, the components of hydraulic conductivity tensor k_{xx}, $k_{yx}=k_{xy}$, and k_{yy} can be derived utilizing the same formula as that used for stress analysis [15]. For a homogenous and anisotropic material, Equation (1) can be further reduced to the following expression for an x', y' co-ordinate system:

$$k_{x'}\frac{\partial^2 h}{\partial x'^2}+k_{y'}\frac{\partial^2 h}{\partial y'^2}=0 \tag{2}$$

The value of PWP u equals $\gamma_w \cdot h_u$, where γ_w is the unit weight of water, and the pressure head h_u can be determined from the relation of $h=h_u+h_z$, where h_z is the elevation head.

Numerical model of groundwater flow in finite slopes with hydraulic conductivity anisotropy

Two-dimensional groundwater flow for an anisotropic finite slope can be derived by numerical methods based on Equation (2). A commercial finite difference code, Fast Lagrangian Analysis of Continua (FLAC) version 4.0, is employed to simulate gravity-driven groundwater flow in a finite slope with hydraulic conductivity anisotropy. In this study, a 7-m-high slope with a 60°

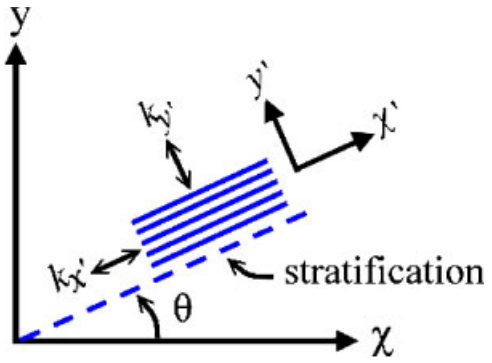

Figure 1. The global and local co-ordinate systems (x,y and x', y').

DOI: 10.1002/nag

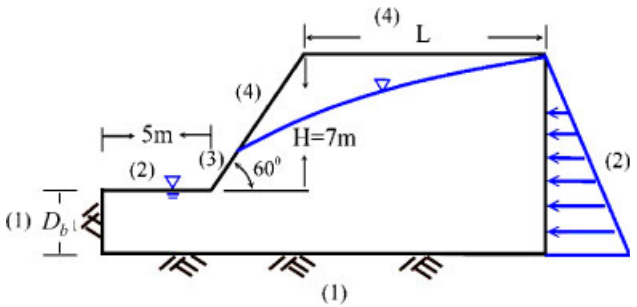

Figure 2. Geometrical and boundary conditions for the modelled finite slope. L is selected as 7 m ($L/H=1$), 14 m ($L/H=2$) or 21 m ($L/H=3$); D_b is selected as 2, 3 or 4 m. (1) *Impervious boundaries*: The gradient of total hydraulic head, i.e, flow velocity, is normal to the boundary at any point must vanish (Neumann boundary). An impervious boundary defines the lowest streamline. (2) *Boundaries of the reservoirs*: PWP along the boundary is taken as hydrostatic. The total hydraulic head on the boundary must be constant (Dirichlet boundary). Boundaries of the reservoirs are equipotential lines. (3) *Surface of seepage*: The pressure along the boundary is taken as atmospheric. Consequently, the total head varies linearly with the elevation head on the boundary. (4) *Free surface*: No seepage occurs along this boundary. The pressure along the boundary is also taken as atmospheric.

inclination was simulated. Figure 2 presents the geometrical and boundary conditions of this numerical model, which is a typical geometry of a slope near a stream. The bottom and left boundaries are assumed to be impermeable. The water table beyond the toe coinciding with the toe level is represented as stream tail water. The top flat surface is free surfaces (no seepage occurs). The slope surface is free surface or surface of seepage. The FLAC algorithms determine the phreatic surface denoting a zero pressure head boundary. A hydrostatic PWP distribution is applied on the right boundary of the proposed model. The right boundary represents a boundary in which the ground water flow is horizontal. When the bottom boundary is assigned as the datum, the total hydraulic head on the right vertical boundary is $H + D_b$. Most boundary conditions in the proposed numerical model are identical to those in the numerical and physical model proposed by Rulon and Freeze [8] with the exception of that the right boundary in Rulon and Freeze's model is an impermeable boundary representing a water divide and the top flat boundary is an infiltration boundary.

VALIDITY OF USING EQUIVALENT ANISOTROPIC HYDRAULIC CONDUCTIVITIES TO MODEL GROUNDWATER FLOW IN A STRATIFIED AND POORLY CEMENTED ROCK SLOPE

Stratified and poorly cemented rock is heterogeneous. To numerically analyse groundwater flow within a slope composed of stratified cemented rock, a dense mesh is required to determine the boundaries of each layer. However, this approach may become intractable and time-consuming when the slope is comprised of alternating beds with many extremely thin layers. When the heterogeneous medium can be replaced by a homogenous medium with anisotropy by introducing a set of overall equivalent hydraulic conductivities, only a low-density mesh is required.

DOI: 10.1002/nag

Figure 3 presents the concept of using an equivalently anisotropic medium to represent a heterogeneous medium (stratified with materials I and II). When the concerned scale is sufficiently large compared with the thickness of layered materials, the heterogeneous medium can be modelled as an equivalently homogenous and anisotropic medium. To validate this notion, a series of two-dimensional groundwater flow analyses were performed for five modelled slopes with different alternating layer thicknesses.

Models (*a*)–(*d*) are presented in the left of Figure 4. The stratified medium comprises several layers of two isotropic materials (Materials I and II) that have the same thickness. The hydraulic conductivities of materials I and II are $k_{\mathrm{I}} = 10^{-5}$ cm/s and $k_{\mathrm{II}} = 10^{-7}$ cm/s, respectively. Thickness of each alternating layer (t) is equal to 2.68, 1.79, 0.89, and 0.45 m for *Models* (*a*)–(*d*), respectively. Theoretically, the equivalent hydraulic conductivities $(k_{x'})_{\mathrm{equi}}$ and $(k_{y'})_{\mathrm{equi}}$ in the principal directions of the stratified medium are directly derived [16] as follows:

$$(k_{x'})_{\mathrm{equi}} = \frac{1}{2 \cdot t}[k_{\mathrm{I}} \cdot t + k_{\mathrm{II}} \cdot t] \tag{3}$$

$$(k_{y'})_{\mathrm{equi}} = \frac{2 \cdot t}{(t/k_{\mathrm{I}}) + (t/k_{\mathrm{II}})} \tag{4}$$

Accordingly, the heterogeneous medium for *Models* (*a*)–(*d*) can be modelled as an equivalently homogenous anisotropic medium with $(k_{x'})_{\mathrm{equi}} = 5.05 \times 10^{-6}$ cm/s and $(k_{y'})_{\mathrm{equi}} = 1.98 \times 10^{-7}$ cm/s. Table I lists input parameters and other related simulation conditions. Figure 4(e) shows the simulated result of an equivalently homogenous and anisotropic model, i.e. *Model* (*e*). The pattern of equipotentials, flow lines and phreatic surfaces of *Model* (*d*) (Figure 4(d)) are similar to those in the equivalently homogeneous anisotropic modelled slope (i.e. *Model* (*e*) in Figure 4(e)). Figure 5(a) shows the difference for PWP in all simulated models, *Models* (*a*)–(*e*), along the grid points of the specified arc (Figure 5(b)). The PWP of *Models* (*b*)–(*d*) along the grid points of the specified arc are essentially identical to that of *Model* (*e*). Based on the equipotentials shown in Figure 4, the boundary effect of each layer on converting a stratified slope with sufficiently thin layer thickness to an equivalently homogeneous slope becomes negligible, especially when only the difference in calculated PWP along a specified arc in the modelled slope is of concern. Therefore, for a stratified heterogeneous rock with a very thin alternating layer that is predominant in the northern section of the outer foothill zone, the process for converting the model of the stratified slope to an equivalently homogeneous and

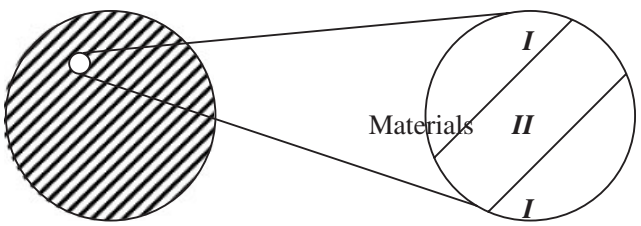

Figure 3. This schematic figure presents the heterogeneous medium comprises of two isotropic materials, I and II. The concerned scale is sufficiently large compared with the thickness of layered materials; the heterogeneous medium (on the right; microview) can be modelled as an equivalently homogenous medium with anisotropy (on the left; macroview).

DOI: 10.1002/nag

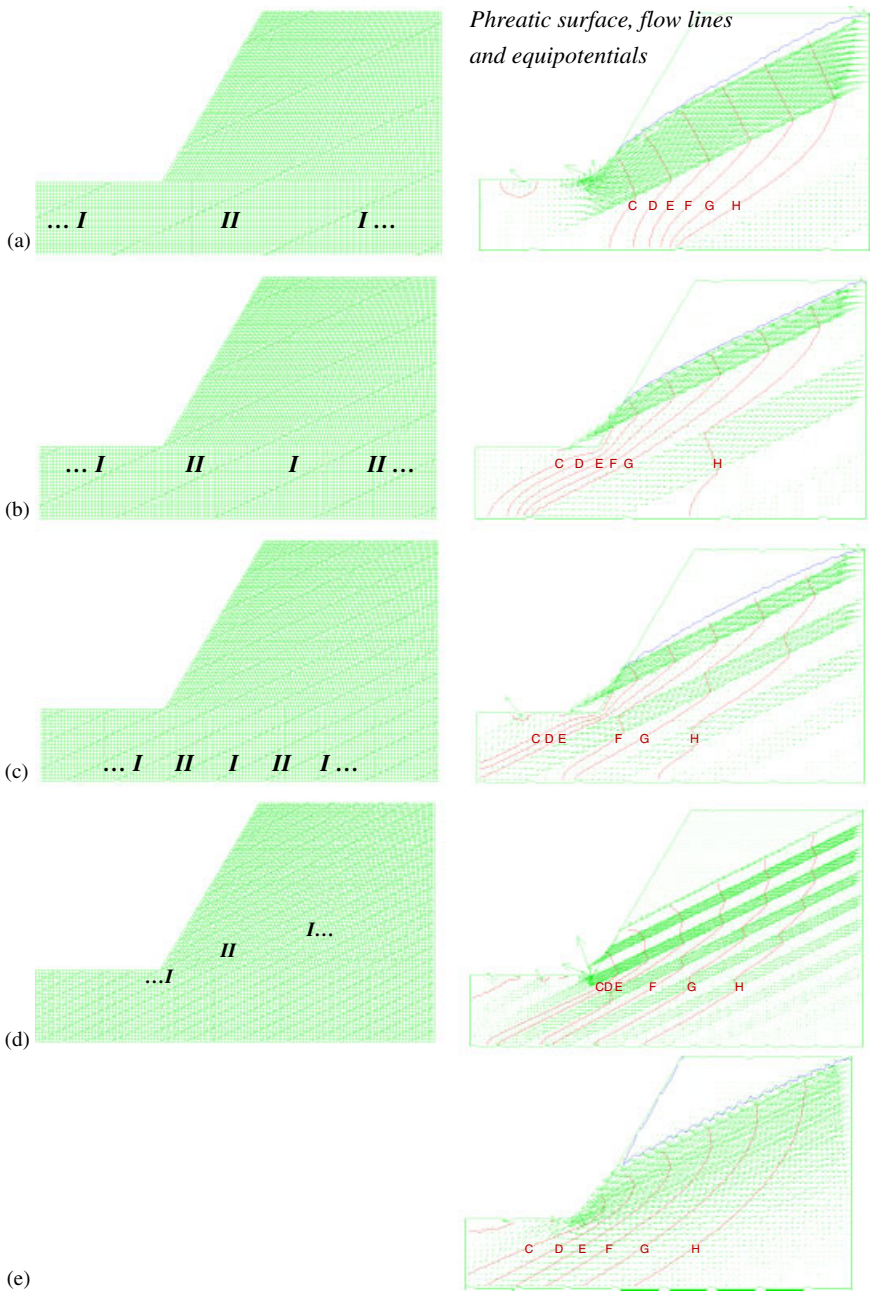

Figure 4. The equipotentials, flow lines and phreatic surfaces for the modelled slopes (L are selected as 7m; $L/H=1$; $D_b = 3$ m). *Models* (*a*)–(*d*) simulate stratified medium comprises several layers of two isotropic materials ($k_{\mathrm{I}} = 10^{-5}$ cm/s and $k_{\mathrm{II}} = 10^{-7}$ cm/s) that have the same thickness. *Model* (*e*) simulates an equivalently homogenous and anisotropic medium. The inclined angle θ is equal to 26.6°. (Total head on equipotential lines C and H is 4 and 9 m, respectively.)

DOI: 10.1002/nag

Table I. Model description and the input hydraulic conductivities for the simulated modelled slopes shown in Figure 4.

The input hydraulic conductivity (cm/s)	The thickness of each alternating layer (m)	The number of alternating layers	The corresponding figure	Model description
Model (*a*)–(*d*)	$t = 2.68$	6	Figure 4(a)	1. The case of heterogeneous stratified medium that is composed of two isotropic materials I and II having the same thickness.
For material I, $k_1 = 10^{-5}$	$t = 1.79$	8	Figure 4(b)	2. A dip slope with its inclined angle θ of the bedding layer equal to 26.6
For material II, $k_{II} = 10^{-7}$	$t = 0.89$	14	Figure 4(c)	3. The geometrical and boundary conditions ($L/H = I$; $D_b = 3m$) are shown in Figure 2.
	$t = 0.45$	27	Figure 4(d)	
Model (*e*) $(k_{x'})_{equal} = 5.05 \times 10^{-6}$ $(k_{y'})_{equal} = 1.98 \times 10^{-7}$	N/A	N/A	Figure 4(e)	1. The case of an equivalently homogeneous and anisotropic medium whose principal directions of hydraulic conductivity tensor are perpendicular and parallel to the bedding plane in *Models* (*a*) through (*d*). 2. The geometrical and boundary conditions ($L/H = I$; $D_b = 3m$) are shown in Figure 2.

anisotropic medium can be utilized for groundwater flow analysis. Hereafter, simulation results are referred to as those for equivalently homogeneous slopes.

PARAMETRIC STUDY FOR PWP DISTRIBUTED IN THE MODELLED FINITE SLOPE WITH HYDRAULIC CONDUCTIVITY ANISOTROPY

This research performed series of parametric studies to assess the influence of hydraulic conductivity anisotropy on PWP distribution in modelled slopes. Different anisotropic ratios $k_{x'}/k_{y'}$ and inclined angles of stratification θ (Figure 1) of the hydraulic conductivity tensors in the modelled slope with $L/H = 1$ and $D_b = 3$ m were adopted for the following simulation. That is, the selected principal values of hydraulic conductivity tensor are (1) $k_{x'} = 10^{-5}$ cm/s and $k_{y'} = 10^{-6}$ cm/s, (2) $k_{x'} = 10^{-5}$ cm/s and $k_{x'} = 10^{-7}$ cm/s, and (3) $k_{x'} = 10^{-5}$ cm/s and $k_{x'} = 10^{-8}$ cm/s. Therefore, the related anisotropic ratios of hydraulic conductivity $k_{x'}/k_{y'}$ are 10, 100, and 1000. The selected inclined angles θ between maximum principal direction of

DOI: 10.1002/nag

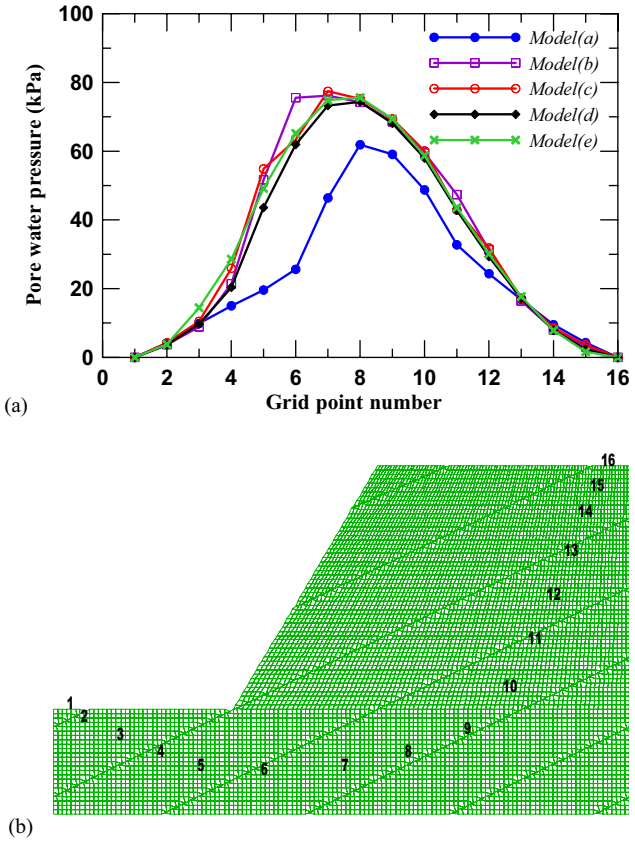

Figure 5. The PWP of all simulated models, *Models* (*a*)–(*e*), along the grid points for the specified arc: (a) the PWP distribution; and (b) locations of grid points along the specified arc.

hydraulic conductivity tensor x' and the x-axis are 0°, $\pm 15^\circ$, $\pm 30^\circ$, $\pm 45^\circ$ and $\pm 60^\circ$. A positive sign for θ denotes the simulated case of a dip slope whose dip direction of stratification is in the same dip direction as the slope. A negative sign for θ indicates the simulated case of an anaclinal slope in which the dip direction of stratification is opposite to the dip direction of the slope. Figure 6 presents the elucidated variables. The input properties for groundwater flow in all simulated cases are as follows: porosity = 0.3; density of water = 1000 kg/m^3; and, bulk modulus of water = 10 kPa. A low bulk modulus of water is adopted to hasten the convergence of calculation in these steady-state simulations.

Groundwater flow pattern and PWP distributed in the modelled slopes

The pattern of groundwater flow in the modelled slope with $L/H = 1$ and $D_b = 3$ m is evaluated. The left part of Figure 7(a) shows the calculated phreatic surface and equipotentials of groundwater flow in the modelled slope with isotropic hydraulic conductivity

DOI: 10.1002/nag

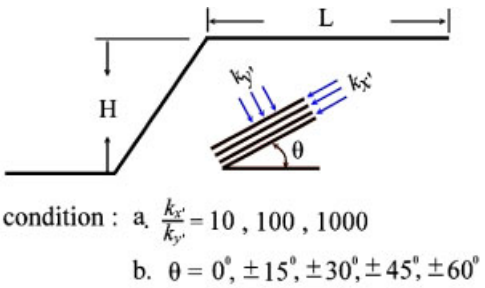

Figure 6. The selected parameters for parametric study for groundwater flow simulation.

($k_{x'}/k_{y'} = 10^{-5}$ cm/s). Figures 7(b) and 7(c) present the phreatic surface and equipotentials of groundwater flow in the modelled slope with the inclined angles $\theta = 0^\circ$ and $\theta = 30^\circ$. The anisotropic ratio of hydraulic conductivity $k_{x'}/k_{y'}$ is 10 ($k_{x'} = 10^{-5}$ cm/s, $k_{y'} = 10^{-6}$ cm/s). The flow patterns (left of Figure 7) are substantially similar to results from physical analogue simulations [17] (reproduced from Reference [18], and right of Figure 7).

The phreatic surface and equipotentials of modelled slope with anisotropic hydraulic conductivity (left of Figure 7(b)) can be calculated by working in a transformed co-ordinate space [16]. An anisotropic slope with an inclined angle $\theta = 0^\circ$ can be transformed into an isotropic slope by retaining the natural y-axis when transforming the x-axis as follows:

$$x' = x \cdot \sqrt{\frac{k_y}{k_x}} \tag{5}$$

The hydraulic conductivity of the transformed isotropic slope is $k_e = \sqrt{k_x \cdot k_y}$. For the transformed slope, $x' = x/\sqrt{10}$ and $k_e = \sqrt{10} \times 10^{-6}$ cm/s since $k_{x'}/k_{y'}$ of the model slope is 10 ($k_{x'} = 10^{-5}$ cm/s, $k_{y'} = 10^{-6}$ cm/s). Figure 8(a) shows the transformed geometry of the model slope and the calculated phreatic surface and equipotentials of groundwater flow with equivalently isotropic hydraulic conductivity. Figure 8(b) shows the phreatic surface and equipotentials of groundwater flow in modelled slope for the untransformed geometry. The anisotropic model is valid since the phreatic surface and equipotentials of groundwater flow (left of Figure 7(b)) are identical with the results obtained using a geometrical transformation approach (Figure 8(b)).

Figures 9–12 show the results of groundwater flow analysis with different anisotropic ratios and the principal directions of the hydraulic conductivity tensor. Figure 9 shows the calculated distribution of PWP and equipotentials for $\theta = 30^\circ$ with the anisotropic ratio of hydraulic conductivity equal to 10 ($k_{x'} = 10^{-5}$ cm/s, $k_{y'} = 10^{-6}$ cm/s). Figure 10 shows the PWP distribution and equipotentials of the anisotropic ratio of hydraulic conductivity equal to 1000 ($k_{x'} = 10^{-5}$ cm/s, $k_{y'} = 10^{-8}$ cm/s) for $\theta = 30^\circ$. Figures 11 and 12 show the calculated distribution of PWP and equipotentials for $\theta = -30^\circ$ (representing an anaclinal slope) with the same hydraulic conductivity as that in Figures 9 and 10, respectively. Based on the flow analysis results shown in Figures 9–12, it can be concluded that hydraulic conductivity anisotropy has a strong affect on the distribution of PWP and equipotentials.

DOI: 10.1002/nag

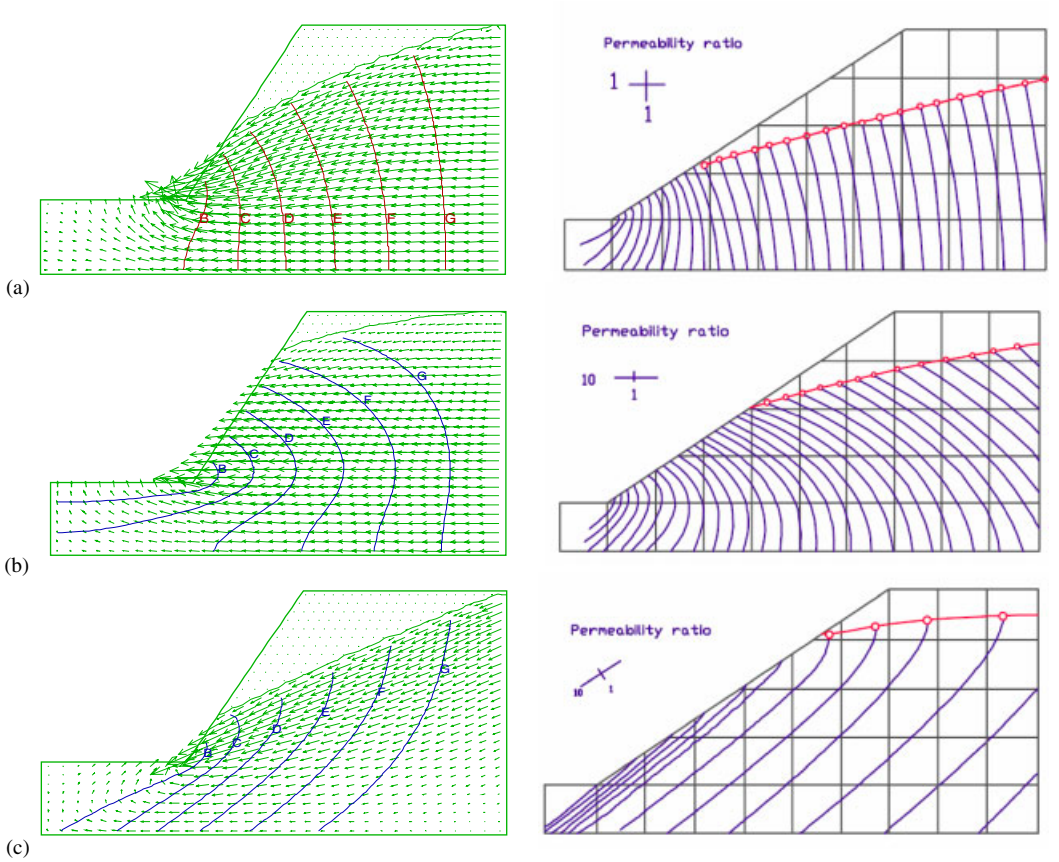

Figure 7. Phreatic surface, flow lines and equipotentials (total head on equipotential lines B and G is 4 m and 9 m) of groundwater flow in the modelled slope (left) with $L/H = 1$ and $D_b = 3$ m and in a finite slope simulated by Sharp *et al.* [17] (right is reproduced from [18]): (a) isotropic slope ($k_{x'} = k_{y'} = 10^{-5}$ cm/s); (b) $k_{x'} = 10^{-5}$ cm/s, $k_{y'} = 10^{-6}$ cm/s with $\theta = 0°$; and (c) $k_{x'} = 10^{-5}$ cm/s and $k_{y'} = 10^{-6}$ cm/s with $\theta = 30°$ (left figure) and an inclined angle identical with the slope angle (right figure).

PWP distributed along a specified arc of the modelled slope

To demonstrate further the influence of hydraulic conductivity anisotropy on PWP distribution in the modelled slope, PWP distributed along a specified arc representing a potential failure surface is derived for different anisotropic ratios and the principal directions of the hydraulic conductivity tensor. As in the previous subsection, the modelled slope with $L/H = 1$ and $D_b = 3$ m is employed. Figure 13 presents the locations of grid points along the specified arc. The values of PWP are presented and discussed as follows.

Figure 14 shows the effect of the inclined angle θ on the PWP distributed along the specified arc of a finite dip slope with $k_{x'}/k_{y'} = 10$ and $k_{x'}/k_{y'} = 1000$. The distribution of PWP for the dip slope with $k_{x'}/k_{y'} = 10$ is not sensitive to the inclined angle θ. Conversely, for the dip slope with $k_{x'}/k_{y'} = 1000$, the PWP is generally inclined to increase as θ decreases (Figure 14(b)).

DOI: 10.1002/nag

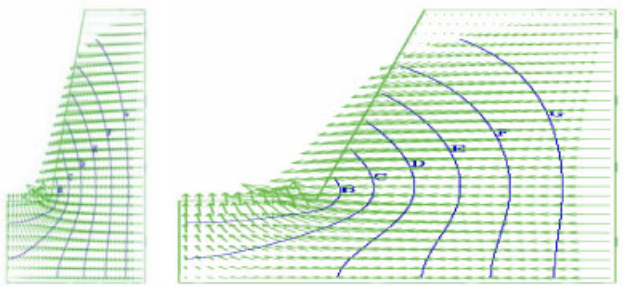

Figure 8. (a) The transformed geometry of the model slope and the calculated phreatic surface and equipotentials of groundwater flow with equivalently isotropic hydraulic conductivity; and (b) the phreatic surface and equipotentials of groundwater flow for the true geometry in natural scale transformed from panel (a).

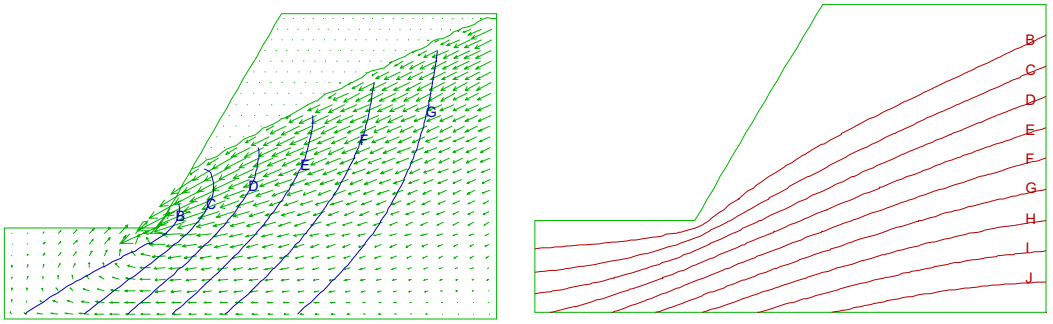

Figure 9. Simulation results for groundwater flow in the modelled dip slope ($L/H = 1$; $D_b = 3$ m) with an inclined angle of stratification $\theta = 30^\circ$ ($k_{x'} = 10^{-5}$ cm/s, $k_{y'} = 10^{-6}$ cm/s): (a) the equipotentials, flow line and phreatic surface; and (b) PWP contours with labels B and J equal to 10 and 90 kPa, respectively.

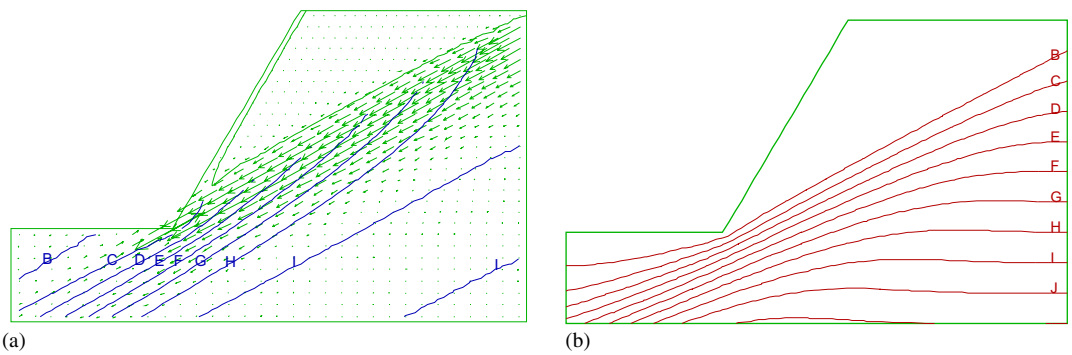

Figure 10. Simulation results for groundwater flow in the modelled dip slope ($L/H = 1$; $D_b = 3$ m) with an inclined angle $\theta = 30^\circ$ ($k_{x'} = 10^{-5}$ cm/s, $k_{y'} = 10^{-8}$ cm/s): (a) the equipotentials, flow line and phreatic surface; and (b) PWP contours with labels B and J equal to 10 and 90 kPa, respectively.

DOI: 10.1002/nag

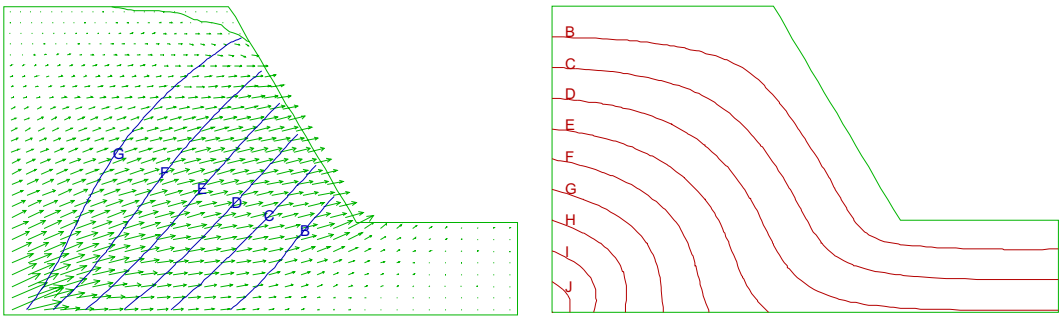

Figure 11. Simulation results for groundwater flow in the modelled dip slope ($L/H = 1$; $D_b = 3$ m) with an inclined angle $\theta = -30^\circ$ ($k_{x'} = 10^{-5}$ cm/s, $k_{y'} = 10^{-6}$ cm/s): (a) the equipotentials, flow line and phreatic surface; and (b) PWP contours with labels B and J equal to 10 and 90 kPa, respectively.

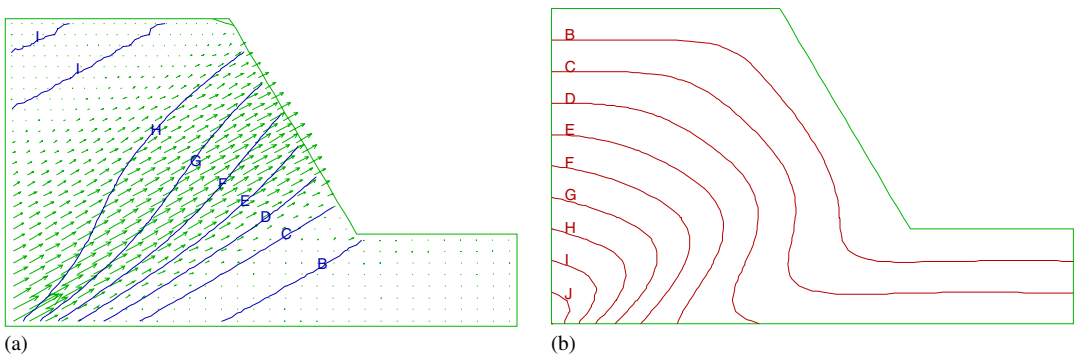

Figure 12. Simulation results for groundwater flow in the modelled dip slope ($L/H = 1$; $D_b = 3$ m) with an inclined angle $\theta = -30^\circ$ ($k_{x'} = 10^{-5}$ cm/s, $k_{y'} = 10^{-8}$ cm/s): (a) the equipotentials, flow line and phreatic surface; and (b) PWP contours with labels B and J equal to 10 and 90 kPa, respectively.

Figure 15 presents the effect of the inclined angle θ on the PWP distributed along the specified arc of a finite anaclinal slope with $k_{x'}/k_{y'} = 10$ and $k_{x'}/k_{y'} = 1000$. For the anaclinal slope the distribution of PWP is not as sensitive to the inclined angle θ as is the dip slope (Figures 15(a) and 15(b)). Figure 16 shows the impact of the anisotropic ratio for hydraulic conductivity $k_{x'}/k_{y'}$ on the PWP distribution for an anisotropic finite slope. In Figure 16(a), the PWP for a dip slope clearly increases as the degree of anisotropy increases. On the other hand, the influence of $k_{x'}/k_{y'}$ on the PWP for anaclinal slopes is less pronounced than that for dip slopes (Figure 16(b)).

INFLUENCE OF HYDRAULIC CONDUCTIVITY ANISOTROPY ON PWP ESTIMATION USING AN EXTRAPOLATION APPROACH

The technique for estimating PWP in a finite slope by defining a hydrostatic phreatic surface is widely used. That is, the PWP at any location in a slope is defined as $\gamma_w \cdot (h_w - z)$ where γ_w is the

DOI: 10.1002/nag

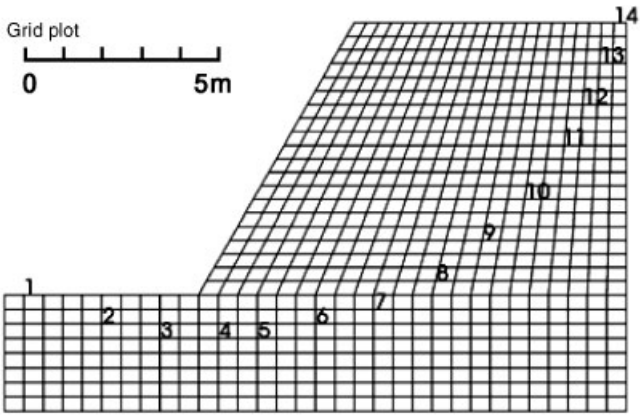

Figure 13. The numbered grid points along the specified arc represent a potential failure surface.

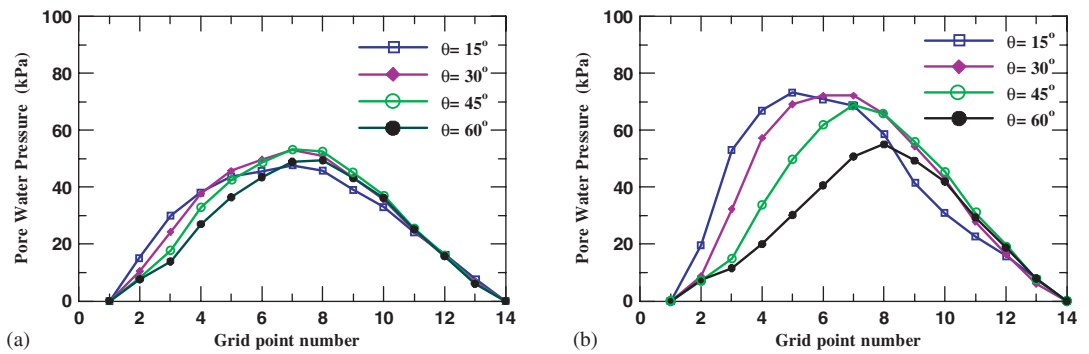

Figure 14. The PWP distribution along the specified arc of the modelled dip slope ($L/H = 1$; $D_b = 3$ m) with an anisotropic ratio of hydraulic conductivity: (a) $k_{x'}/k_{y'} = 10$; and (b) $k_{x'}/k_{y'} = 1000$.

unit weight of water and $(h_w - z)$ is the vertical distance from a location (elevation equals z) to the phreatic surface. The phreatic surface of a finite slope can be obtained according to measured water tables in open standpipes at various field locations. Because extensive field data is not always available, the phreatic surface is usually extrapolated based on limited field data. According to Dupuit's theory (Figure 17), the phreatic surface in a homogenous isotropic slope can be derived approximately when water table heights at two fixed points (e.g. locations of head and tail water) are known [19]. Therefore, the required PWP distribution for slope stability analysis can be simply derived from the inferred phreatic surface. The technique for estimating PWP by extrapolating a phreatic surface based on isotropic Dupuit's theory and assuming the pore pressure under the inferred phreatic surface is called the extrapolating approach hereafter.

Lorig [20] indicated that in a slope stability analysis for a homogeneous isotropic slope, no significant difference exists between the PWP distribution estimated by defining a hydrostatic

DOI: 10.1002/nag

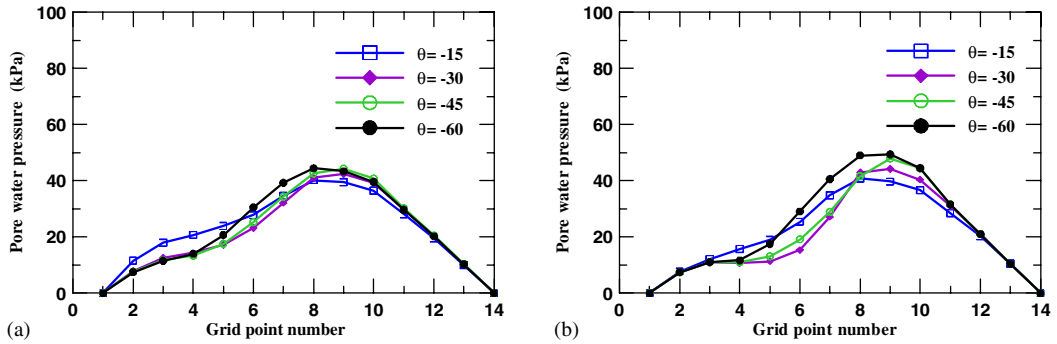

Figure 15. The PWP distribution along the specified arc of the modelled anaclinal slope ($L/H = 1$; $D_b = 3$ m) with an anisotropic ratio of hydraulic conductivity: (a) $k_{x'}/k_{y'} = 10$; and (b) $k_{x'}/k_{y'} = 1000$.

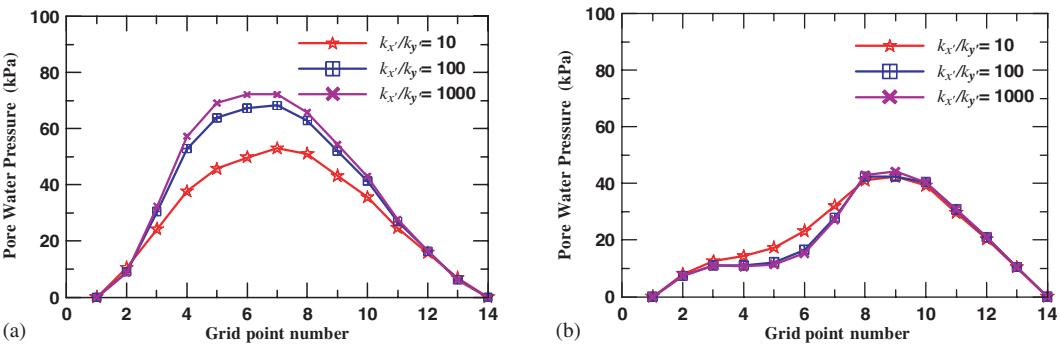

Figure 16. The PWP distribution along the specified arc of the modelled slope ($L/H = 1$; $D_b = 3$ m) with anisotropic ratios of hydraulic-conductivity: $k_{x'}/k_{y'} = 10$, 100, and 1000: (a) a dip slope with an inclined angle $\theta = 30^\circ$; and (b) anaclinal slope with an inclined angle $\theta = -30^\circ$.

phreatic surface and those acquired from a complete groundwater flow analysis. However, it is debatable whether this conclusion is valid for a stratified and poorly cemented rock slope with anisotropic hydraulic conductivity. To determine the validity of this conclusion for anisotropic rock slope, the computed PWPs derived from the extrapolating approach and from a complete groundwater flow analysis along the specified arc (Figure 13) are compared. The two solid lines in Figure 18 represent the PWP distributed in the modelled slope ($L/H = 1$; $D_b = 3$ m) with isotropic hydraulic conductivity. In a finite isotropic slope then, the PWP obtained from the groundwater flow analysis with FLAC algorithms (solid line with triangles) is roughly identical to the PWP obtained using the extrapolating approach (solid line with squares). The total value of PWP based on the extrapolating approach was only 7% less than that obtained by isotropic groundwater flow analysis.

Figure 18 also shows that the actual PWP in the modelled slope with hydraulic conductivity anisotropy (dash lines) deviates from the estimated PWP in the modelled slope with hydraulic

DOI: 10.1002/nag

conductivity isotropy (solid lines). The difference between PWP derived from flow analysis and extrapolating approach increases as the degree of anisotropy increases both in a dip and anaclinal slope ($\theta = 30^\circ$ and -30°) under given boundary conditions. For dip slopes with $k_{x'}/k_{y'} = 10$ and $k_{x'}/k_{y'} = 1000$, the total value of PWP for all grid points along the specified arc were 34 and 76%, respectively, greater than that obtained using the extrapolating approach (solid line with squares). For anaclinal slopes with $k_{x'}/k_{y'} = 10$ and $k_{x'}/k_{y'} = 1000$, the total values for PWP along the specified arc were 2 and 8%, respectively, less than that obtained utilizing the extrapolating approach. That is, applying the extrapolating approach to calculate the PWPs in an anisotropic rock slope, especially for a dip slope, leads to considerable errors.

To assess the impact of hydraulic conductivity anisotropy and boundaries for the modelled slope on the estimation of PWPs using the extrapolation approach, the groundwater flow in the modelled slope with different $k_{x'}/k_{y'}$, θ, L/H and D_b was simulated. To represent the ratio of PWP derived from flow analysis and extrapolation approach, a correction factor $C_{\text{ani/iso}} = \Sigma\text{PWP}_{\text{(flow analysis)}}/\Sigma\text{PWP}_{\text{(extrapolation approach)}}$ is introduced. Notably, ΣPWP is the summed PWPs for 14 grid points along the specified arc in the modelled slope (Figure 13). The $\Sigma\text{PWP}_{\text{(flow analysis)}}$ and $\Sigma\text{PWP}_{\text{(extrapolation approach)}}$ represent ΣPWP derived from groundwater flow analysis and that using the extrapolation approach. The correction factor $C_{\text{ani/iso}}$ greater/less than 1 suggests that PWPs will be underestimated/overestimated when an extrapolation approach is utilized. Figures 19 and 20 show the calculated correction factor $C_{\text{ani/iso}}$. Generally, PWPs are underestimated when an anisotropic slope is simplified as an isotropic slope and the extrapolation approach is adopted.

Figures 19(a)–(c) show $C_{\text{ani/iso}}$ for an anisotropic slope with $k_{x'}/k_{y'} = 10$ and $D_b = 3$. The correction factor $C_{\text{ani/iso}}$ increases as $k_{x'}/k_{y'}$ increases. Figure 19(b) shows $C_{\text{ani/iso}}$ for an anisotropic slope with $k_{x'}/k_{y'} = 100$ (a representative value of thin alternating beds of shale and sandstone). Notably, $C_{\text{ani/iso}}$ is 164−220%, 166−223% and 149−175% when $\theta = 0$, 15 and 30°. That is, the PWP for a modelled dip slope with $k_{x'}/k_{y'} = 100$ and with gently dip angle will be significantly underestimated when using the extrapolation approach. For example, the simulated slope under the given boundary conditions with $L/H = 3$ and $D_b = 3$ m, the ΣPWP

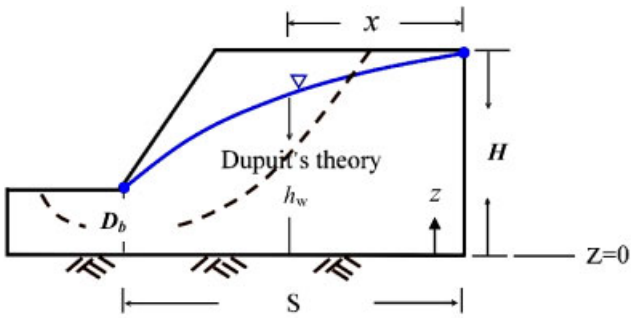

Figure 17. Phreatic surface defined by Dupuit's theory for a homogeneous isotropic slope.

DOI: 10.1002/nag

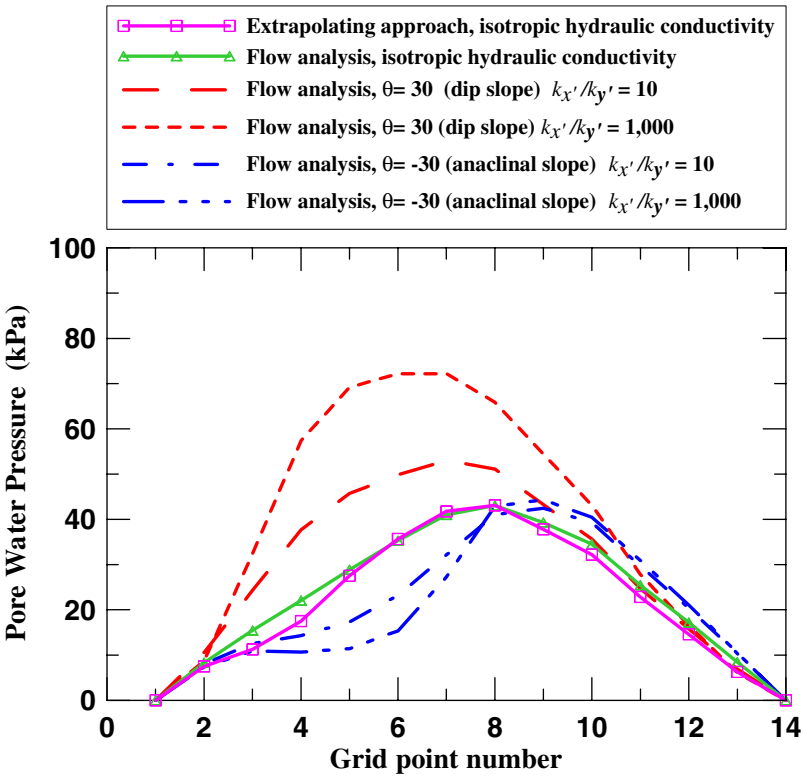

Figure 18. The estimated PWP at the grid points along the specified arc shown in Figure 13 in the isotropic (solid lines) and anisotropic (dashed lines) modelled slope ($L/H = 1$; $D_b = 3$ m) based on complete groundwater flow analysis using the FLAC algorithm and by defining a hydrostatic phreatic surface using Dupuit's theory (extrapolation approach).

are underestimated by 55% when the modelled anisotropic slope with $k_{x'}/k_{y'} = 100$ and $\theta = 15^\circ$ is simplified as isotropic slope and the extrapolation approach is adopted. The PWP for a modelled slope with $k_{x'}/k_{y'} = 100$ is only slightly underestimated to slightly overestimated for an anaclinal slope with a dipping angle $> 15^\circ$ and a dip slope with a dipping angle $> 45^\circ$.

Figures 19(a)–(c) present the effects of L/H on the values of correction factor $C_{\text{ani/iso}}$. The effects of L/H on $C_{\text{ani/iso}}$ is insignificant when $k_{x'}/k_{y'} = 10$ (Figure 19(a)). When $k_{x'}/k_{y'}$ is increased, the effects of L/H on the correction factor $C_{\text{ani/iso}}$ also increases, (Figures 19(a)–8(c)). Figures 20(a)–(c) show the correction factor $C_{\text{ani/iso}}$ for a slope with $L/H = 1$ and $D_b = 2$, 3 and 4m. Compared with the influence of L/H on $C_{\text{ani/iso}}$, D_b has a minor effects on the correction factor $C_{\text{ani/iso}}$.

Based on these modelling results, the PWP along the potential surface obtained using the phreatic surface extrapolated from water tables measured at two standpipes is underestimated markedly for an anisotropic slope, especially for a dip slope with small dip angle. Furthermore, defining a phreatic surface of layered slopes simply based on limited field data is difficult [21].

DOI: 10.1002/nag

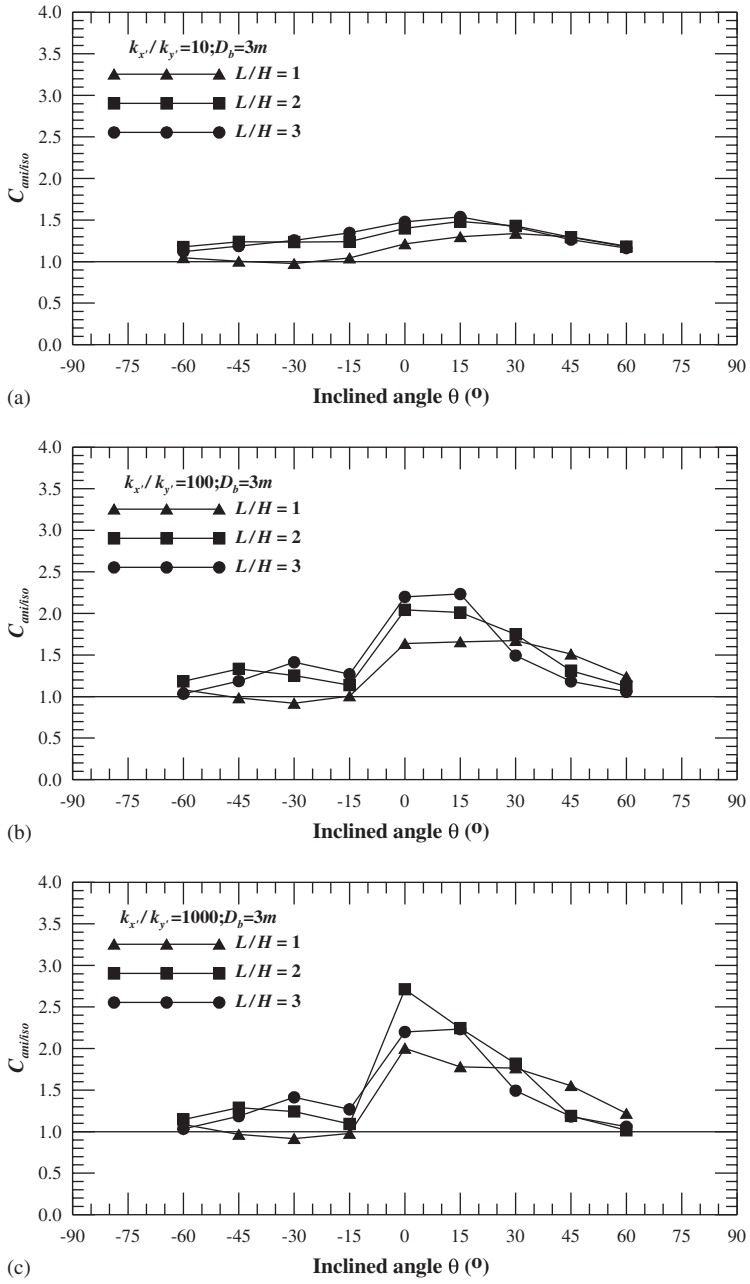

Figure 19. Differences in PWPs derived using the extrapolation approach and from a complete groundwater flow analysis using the FLAC algorithm for modelled slopes with $L/H = 1$, 2, 3, $D_b = 3$ m and (a) $k_{x'}/k_{y'} = 10$; (b) $k_{x'}/k_{y'} = 100$; and (c) $k_{x'}/k_{y'} = 1000$.

DOI: 10.1002/nag

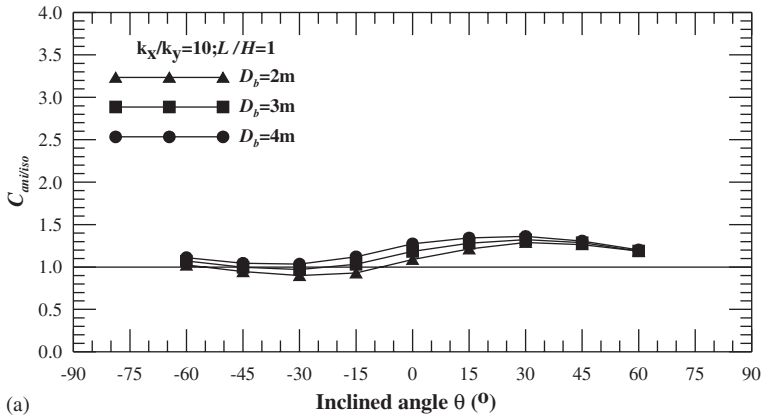

(a)

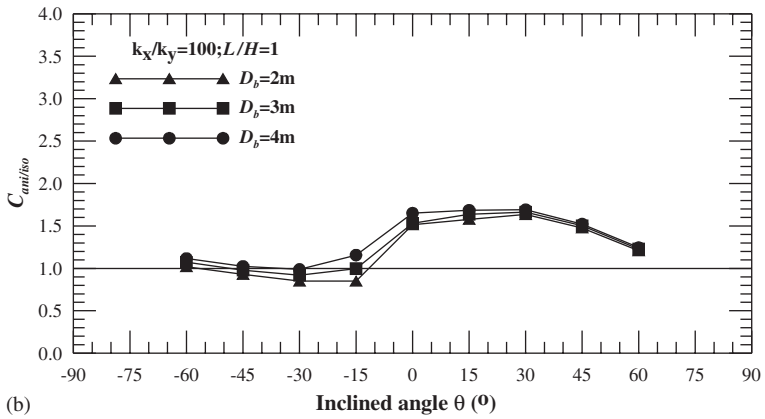

(b)

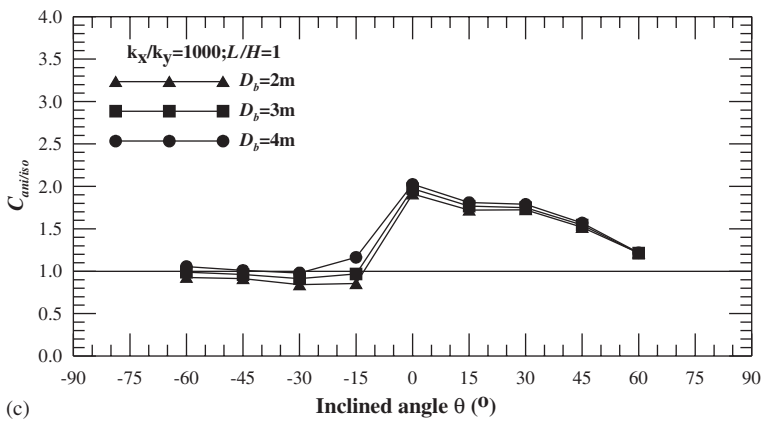

(c)

Figure 20. Differences in PWPs derived using the extrapolation approach and from a complete groundwater flow analysis using the FLAC algorithm for modelled slopes with $D_b = 2$, 3, 4m, $L/H = 1$ and (a) $k_{x'}/k_{y'} = 10$; (b) $k_{x'}/k_{y'} = 100$; and (c) $k_{x'}/k_{y'} = 1000$.

DOI: 10.1002/nag

Therefore, a groundwater flow analysis is necessary when estimating PWP distributed in a stratified and poorly cemented rock slope with hydraulic conductivity anisotropy.

INFLUENCE OF HYDRAULIC CONDUCTIVITY ANISOTROPY ON THE STABILITY OF A FINITE SLOPE

The impact of hydraulic conductivity anisotropy on PWP distribution in a finite slope has been elucidates. The stability of a stratified and poorly cemented rock slope is simulated to investigate the effect of hydraulic conductivity anisotropy. A mechanical analysis was conducted after groundwater flow analysis to determine the stability of the modelled slope with $L/H = 2$ and $D_b = 3$ m. For the mechanical analysis, two vertical boundaries were fixed in the horizontal direction and free in the vertical direction; the bottom boundary was fixed in both directions. Strength reduction technique [22,23] was adopted for calculating the safety factor, in which the Mohr–Coulomb failure criterion was assumed for the modelled stratified, poorly cemented rock slope with its cohesion and friction angle equal to 30 kPa and 32°, respectively. The other input properties of the stratified, poorly cemented rock slope for the mechanical analysis through all simulated cases were density $= 1850\,\mathrm{kg/m^3}$, and shear modulus and bulk modulus are 300 and 900 MPa, respectively.

Figures 21–23 present the PWP and maximum shear strain contours of simulated finite slopes, in which the maximum shear strain is the calculated shear strain at the time step just prior to an extremely large increase in slope displacement occurs. The failure surface — which is referred to as the surface with concentrated density contour of shear strain hereafter—of the isotropic slope is relatively shallow (Figure 21(b)) compared to that of the anisotropic slope (Figure 22(b)) with an anisotropic ratio of hydraulic conductivity $k_{x'}/k_{y'} = 100$ and $\theta = 30^\circ$ (dip slope). The calculated safety factors for both the modelled slopes shown in Figure 21 and Figure 22 are 2.0. Notably, the currently selected domain for mechanical analysis may be insufficiently large to eliminate the boundary constraint on the development of the failure surface (Figure 22(b)). However, the simulated results still revealed that the effect of the hydraulic conductivity anisotropy on the PWP has a significant influence on effective normal stress and, thus, shear strength along the failure surface.

Figure 23 shows the PWP and maximum shear strain contours for a simulated finite slope with an anisotropic ratio of hydraulic conductivity $k_{x'}/k_{y'} = 100$ and $\theta = -30^\circ$ (anaclinal slope). In this case, the pattern of the failure surface of the simulated anisotropic finite slope is roughly identical to that for the simulated isotropic slope. It is notable that the shear strain level for the anisotropic anaclinal slope (Figure 23) is greater than the one for the isotropic slope (Figure 21). Additionally, the safety factor for the anisotropic finite anaclinal slope (Figure 23) is 1.7, rather than 2.0, the safety factor for the isotropic slope (Figure 21) and dip slope (Figure 22). Accordingly, hydraulic conductivity anisotropy and different principal directions of hydraulic conductivity tensor result in different depths of failure surfaces, levels of shear strain and safety factors in the modelled anisotropic slopes. The surfaces with concentrated density contour of shear strain (Figures 21–23) are circular surfaces. However, plane failure along the bedding plane is also possible for a dip slope composed of stratified and poorly cemented rock. Furthermore, thin alternating beds of shale and sandstone can possess strength anisotropy. Strength anisotropy can affect the safety factor and shape of failure surface. Coupling effect of strength and hydraulic conductivity anisotropy in a stratified and poorly cemented rock slope

DOI: 10.1002/nag

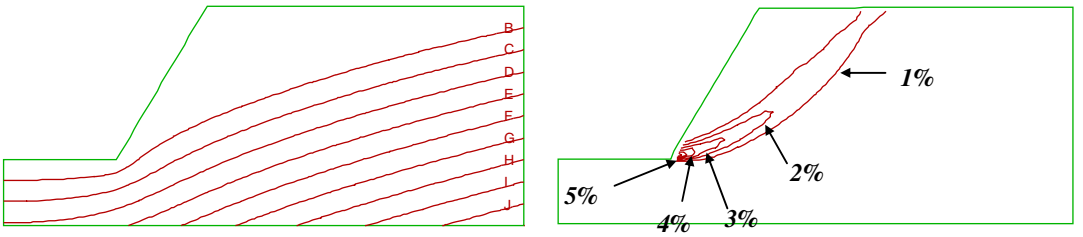

Figure 21. The PWP and the related maximum shear strain contours for a finite slope ($L/H = 2$; $D_b = 3$ m) with an isotropic hydraulic conductivity: (a) PWP contours for groundwater flow. The PWP on B and J are 10 and 90 kPa, respectively; and (b) the maximum shear strain contours obtained from stability analysis. The safety factor for the modelled isotropic slope is 2.0.

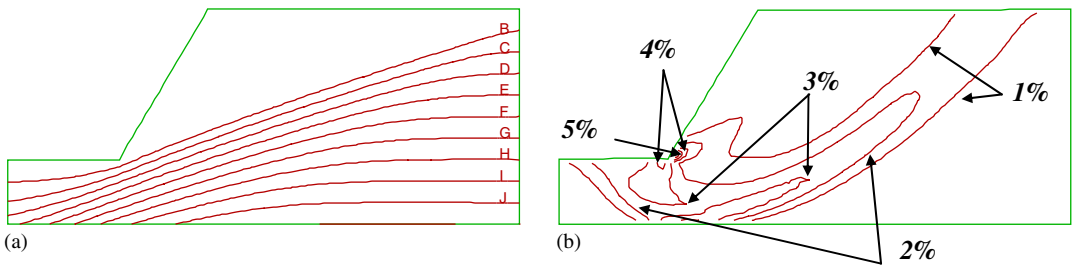

Figure 22. The PWP and the related maximum shear strain contours for a finite dip slope ($L/H = 2$; $D_b = 3$ m) with an anisotropic ratio of hydraulic conductivity $k_{x'}/k_{y'} = 100$ and $\theta = 30°$: (a) The PWP contours for groundwater flow. The PWP on B and J are 10 and 90 kPa, respectively; and (b) the maximum shear strain contours acquired by stability analysis. The safety factor for the modelled dip slope is 2.0.

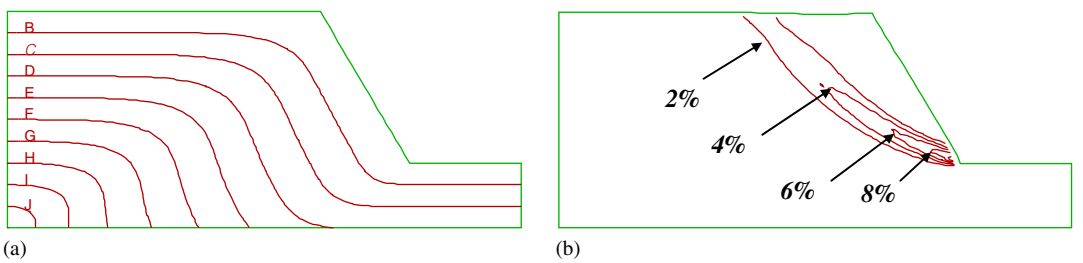

Figure 23. The PWP and related maximum shear strain contours for a finite anaclinal slope ($L/H = 2$; $D_b = 3$ m) with an anisotropic ratio of hydraulic conductivity $k_{x'}/k_{y'} = 100$ and $\theta = -30°$: (a) the PWP contours of groundwater flow. The PWP on B and J are 10 and 90 kPa, respectively; and (b) the maximum shear strain contours acquired by stability analysis. The safety factor for the modelled anaclinal slope is 1.7.

accounts for the affect of a weak plane (bedding plane) on dip slope stability needs to further investigation.

The locations of the failure surfaces and the PWP along the failure surfaces of three modelled slopes (Figures 21–23) are presented in Figure 24. For each case, the so-called grid point

DOI: 10.1002/nag

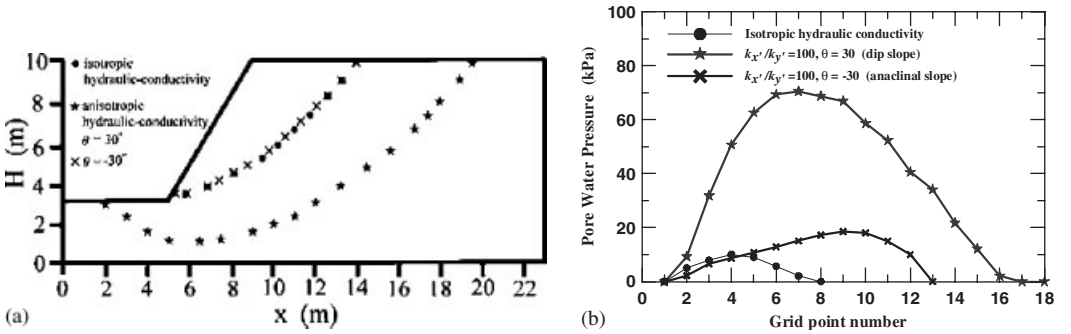

Figure 24. Locations of failure surfaces and the PWP along the failure surfaces for the three modelled slopes shown in Figures 21–23: (a) location of the failure surface; and (b) the PWPs along the grid points of the failure surface shown in panel (a).

numbers shown on the x-axis in Figure 24(b) are sequentially numbered according to the x co-ordinate for corresponding failure surface of model slopes, which is denoted by a series of discrete points (Figure 24(a)). The PWP along the potential failure surface is significantly affected by the hydraulic conductivity anisotropy and the principal directions of the hydraulic conductivity tensor. Consequently, the hydro-geological conditions, including the anisotropic hydraulic characteristics of a stratified and poorly cemented rock slope, should be fully analysed during slope stability analysis.

CONCLUSION

1. The utility of representing a heterogeneous medium as an equivalent anisotropic medium for groundwater flow analysis in a finite slope was examined. For thin alternating beds of stratified, poorly cemented rock slope, ground water flow can be modelled using equivalently homogeneous, anisotropic hydraulic conductivity.
2. The influence of hydraulic conductivity anisotropy on groundwater flow analysis for finite slopes was identified. Simulation results proved that the PWP distribution was substantially different for finite slopes with different hydraulic conductivity anisotropy and different principal directions of hydraulic conductivity tensor. Consequently, hydraulic conductivity anisotropy also strongly governs the groundwater flow in a stratified and poorly cemented rock slope.
3. Estimating PWP distributed in the modelled anisotropic slope using a phreatic surface with isotropic and hydrostatic assumptions generates marked errors, especially for a dip slope with small dip angle. Numerical experiments suggested that this error increased as degree of anisotropy, both for a dip and anaclinal slope, increased. Furthermore, simulated results indicate that the influence of model boundaries on the estimation of PWPs using an extrapolating approach also increased as the degree of anisotropy increased. Consequently, extrapolating PWP based on limited water table measurements and an isotropic model for a stratified, poorly cemented rock slope is inappropriate.
4. Slope stability analysis incorporated with the PWP distribution based on the anisotropic groundwater flow analysis results was performed to demonstrate how anisotropic

DOI: 10.1002/nag

flow affected slope stability. Stability analysis results indicated that hydraulic conductivity anisotropy influenced the slope safety factor and the slip surface pattern. Consequently, we strongly recommended that slope stability analysis for a stratified, poorly cemented rock slope should include groundwater flow analysis that considers hydro-geological conditions.

ACKNOWLEDGEMENTS

The authors would like to thank the National Science Council of the Republic of China, Taiwan for financially supporting this research under Contract No. NSC-91-2211-E-008-024.

REFERENCES

1. Ho CS. 1988. *An Introduction to the Geology of Taiwan Explanatory Text of the Geologic Map of Taiwan* (2nd edn). Central Geological Survey: Taiwan.
2. Yen TL, Chen CH, Chin CT. Case histories of stabilization of highway slopes in soft sandstone and mudstone interbedded formation. *Journal of Sino-geotechnics* 1999; **72**:13–22 (in Chinese).
3. Misfeldt GA, Sauer EK, Christiansen EA. The Hepburn landslide: an interactive slope-stability and seepage analysis. *Canadian Geotechnical Journal* 1991; **28**:556–573.
4. Ku CS, Lee DH. Drilled shafts bearing capacity soft rock. *Journal of Sino-geotechnics* 2004; **99**:93–102 (in Chinese).
5. Biq C. Dual-trench structure in the Taiwan-Luzon region. *Proceedings of the Geological Society of China* 1972; **15**: 65–75.
6. Brace WF. Permeability of crystalline and argillaceous rocks. *International Journal of Rock Mechanics and Mining Sciences and Geomechanics Abstracts* 1980; **17**:241–251.
7. Tzeng JH. The distribution of pore water pressure in soft rock slope with hydraulic conductivity anisotropy. *M.S. Thesis*, National Central University, Taiwan, R.O.C. 2004, (in Chinese).
8. Rulon JJ, Freeze RA. Multiple seepage faces on layered slopes and their implications for slope-stability analysis. *Canadian Geotechnical Journal* 1985; **22**:347–356.
9. Rulon JJ, Rodway R, Freeze RA. The development of multiple seepage faces on layered slopes. *Water Resources Research* 1985; **21**(11):1625–1636.
10. Iverson RM, Major JJ. Groundwater seepage vectors and the potential for hillslope failures and debris flow mobilization. *Water Resources Research* 1986; **22**(11):1543–1548.
11. Iverson RM. Groundwater flow field in infinite slopes. *Geotechnique* 1990; **40**(1):139–143.
12. Iverson RM, Reid ME. Gravity-driven groundwater flow and slope failure potential 1. Elastic effective-stress model. *Water Resources Research* 1992; **28**(3):925–938.
13. Reid ME, Iverson RM. Gravity-driven groundwater flow and slope failure potential 2. Effects of slope morphology, material properties, and hydraulic heterogeneity. *Water Resources Research* 1992; **28**(3):939–950.
14. Reid ME. Slope instability caused by small variations in hydraulic conductivity. *Journal of Geotechnical and Geoenvironmental Engineering* (ASCE) 1997; **123**(8):717–725.
15. Zienkiewicz OC, Mayer P, Cheung YK. Solution of anisotropic seepage by finite elements. *Journal of Engineering Mechanics* (ASCE) 1966; **92**(EM1):111–120.
16. Terzaghi K, Peck RB, Mesri G. *Soil Mechanics in Engineering Practice*. Wiley: New York, 1996.
17. Sharp JC, Maini YN, Harper TR. Influence of groundwater on the stability of rock masses. *Transactions of the Institute Mining and Metallurgy*, Vol. 81, Bulletin No.782; London, 1972:A13–20.
18. Hoek E, Bray J. *Rock Slope Engineering* (3rd edn). Institution of Mining and Metallurgy: London, 1981; 127–148.
19. Harr ME. *Groundwater and Seepage*. Mcgraw-Hill Book Company: New York, 1962.
20. Lorig L. Lesson learned from slope stability studies. In *FLAC and Numerical Modeling in Geomechanics. Proceedings of the 1st International FLAC Symposium*, Detoumay C, Hart R (eds). Balkema: Rotterdam, 1999; 17–21.
21. Skempton AW, Brown JD. A landslide in boulder clay at Selsect, Yorkshire. *Geotechnique* 1961; **11**:280–293.
22. Dawson EM, Roth WH, Drescher A. Slope stability analysis by strength reduction. *Geotechnique* 1999; **49**(6): 835–840.
23. Mastui T, San KC. Finite element slope stability analysis by shear strength reduction technique. *Soils and Foundation* 1992; **32**(1):59–70.

DOI: 10.1002/nag